ORIGINAL ARTICLE

Effects of hygrothermal aging on the physicochemical and mechanical properties of 3D-printed PA6

Mohammadali Shirinbayan[1] · Khaled Benfriha[2] · Mohammad Ahmadifar[2] · Clara Penavayre[1] · Samia Nouira[1] · Joseph Fitoussi[1]

Abstract

This paper investigates the effects of hygrothermal aging on PA6 filaments used as raw material in fused filament fabrication (FFF). The filaments were subjected to various aging conditions to evaluate their physicochemical and thermomechanical properties. The results show that water was uniformly absorbed at all aging temperatures, although the kinetics of absorption varied. The introduction of water caused an increase in chain mobility, resulting in a decrease in the glass transition temperature, crystallinity, Young's modulus, tensile strength, and yield strength. These changes in properties followed a consistent trend, with an initial rapid decrease followed by stabilization at a minimum value common to all temperatures. Notably, elongation at break increased sevenfold at the highest temperature. Compared to samples printed with unaged filaments, those produced with aged filaments exhibited a decrease in mechanical properties.

Keywords Hygrothermal aging · PA6 · Fused filament fabrication · Mechanical properties

1 Introduction

The demand for the employment of polymer materials in different industries is increased due to their exceptional properties [1–3]. It exists a lot of different manufacturing processes capable of processing polymer objects, but one of the most attractive ones is additive manufacturing (AM). AM is a is a family of technologies that involves layer-by-layer material deposition [4–6]. Seven types of AM systems are defined by the ISO/ASTM 52900:2015 standard. These include material jetting (MJ), binder jetting (BJ), sheet lamination (SL), vat photopolymerization (VP), powder bed fusion (PBF), directed energy deposition (DED), and material extrusion (ME) [7]. The characteristics of each AM method vary in terms of production speed, actual costs, and resolution [8]. As one of the most popular ME techniques, fused filament fabrication (FFF) involves selectively depositing the thermoplastic polymer/composite through heated nozzle(s) [9].

The FFF process is a widely used fabrication technique due to its simple and cost-effective process, economic accessibility, reliability, and ability to manufacture complex shapes with various materials [10, 11]. Various materials possessing various properties and characteristics such as polylactic acid (PLA), acrylonitrile butadiene styrene (ABS), polyetheretherketone (PEEK), polyethylene terephthalate glycol (PETG), polycaprolactone (PCL), polycarbonate (PC), polypropylene (PP), various types of polyethylene (PE), polymethyl methylacrylate (PMMA), and polyamide (PA) are applied in FFF process [12]. Moisture can significantly influence the nylons, especially PA6, due to the hydrophilic feature of the amide functional groups. This feature of PA6 caused great challenges in the technical applications of this polymer for designers. Therefore, numerous

✉ Mohammadali Shirinbayan
Mohammadali.Shirinbayan@ensam.eu

Khaled Benfriha
Khaled.Benfriha@ensam.eu

Mohammad Ahmadifar
Mohammad.Ahmadifar@ensam.eu

Clara Penavayre
Clara.Penavayre@ensam.eu

Samia Nouira
Samia.Nouira@ensam.eu

Joseph Fitoussi
Joseph.Fitoussi@ensam.eu

[1] Arts Et Metiers Institute of Technology, CNRS, CNAM, PIMM, HESAM University, 75013 Paris, France

[2] Arts Et Metiers Institute of Technology, CNAM, LCPI, HESAM University, 75013 Paris, France

studies concerning the durability of polyamides have been conducted [13–17]. Moisture absorbed by polymer materials, particularly PA, leads to changes in their chemical and physical properties. Indeed, PA is a thermoplastic polymer with the repeating group of [—NH(CH_2)$_5$(CO) -] and polar amide groups. The water molecule (H_2O) absorbed during hygrothermal conditioning replaces the existing inter-chain amide-amide bonds with amide-water bonds (Fig. 1) [18, 19]. Therefore, the presence of water can disrupt the pre-existing bond between the C = O and –NH groups within the polymer, causing the loss of its mechanical cohesion [20–22]. In hydrothermal aging, plasticization and swelling are reported as the most significant physical changes resulting from the interaction of water molecules with hydrogen bonds [23].

Puffr and Sebenda [24] suggested a mechanism of water sorption into PA6. This hypothesis conjectures that water penetrates PA by establishing hydrogen bonds between two adjacent amide groups, resulting in three different types of bonding of water molecules (Fig. 2). The following proposed water sorption mechanism does not consider capillary condensation. A double H bond is established between CO groups. As a result of this step, a substantial amount of heat is generated. This water may be categorized as firmly bound water that exhibits a low rate of activity. Furthermore, a double H bond is formed between CO and NH groups as the other two loosely bound molecules with an insignificant thermal effect, which can be easily eliminated via drying [24–26].

Shi et al. [27] conducted a study on the structure and hygrothermal stability of highly oriented PA6 that was manufactured through the solid hot stretching. According to the findings, the molecular orientation was effective to decrease the hydrophilicity of PA6. Consequently, the water uptake and the subsequent molecular hydrolytic degradation were restricted. Kehrer et al. [28] studied the thermoviscoelastic behavior of PA6 concerning the two considered equilibrium moisture contents.

The hygrothermal effects on linear viscoelastic material properties and the onset of mechanical nonlinearity under hygrothermal conditions were evaluated by the authors. Polymers tend to absorb water through their amorphous regions, which affects their chemical, mechanical, and physical properties. [21, 22, 29]. Ksouri et al. [30] investigated these properties to evaluate the impact of the hygrothermal aging on PA6. Aging was conducted in distilled water (pH ≈ 6; 100% RH) at 30 °C, 50 °C, 70 °C, and 90 °C for 80 days. Particularly at high temperatures, several surface damages were recorded, including crazing and yellowness. During aging, the glass transition temperature (T_g) drops

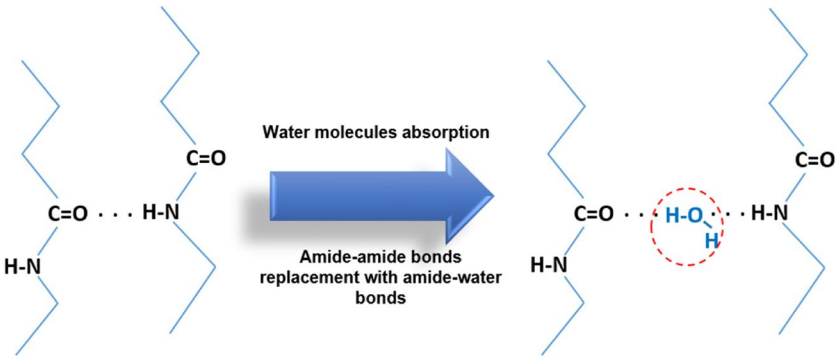

Fig. 1 Water/moisture absorption mechanism concerning the PA6

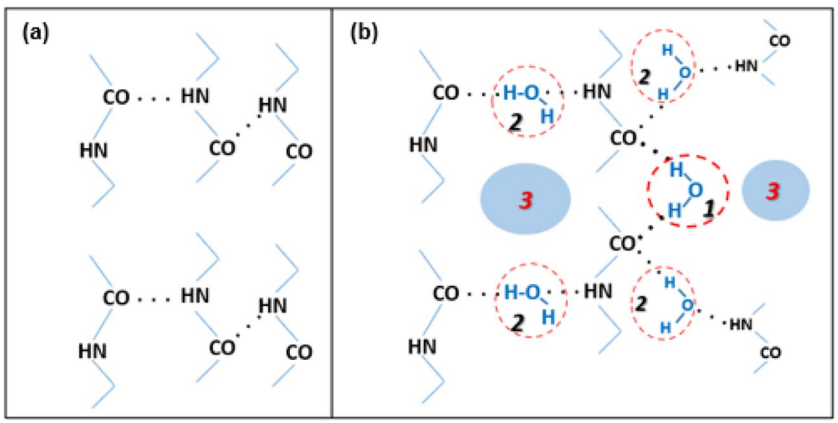

Fig. 2 Mechanism of water sorption in nylon as reported by Puffr and Sebenda: a dry amorphous nylon and b moisturized nylon: (1) firmly bound water; (2) loosely bound water; and (3) sites for capillary condensed water (adapted from ref. 24)

progressively with increasing temperature to reach the lowest value for samples aged at 90 °C. Moreover, a similar tendency was observed in the Young's modulus, the tensile strength, and the elongation at break of the materials studied. Furthermore, the crack formation on the polymer as the consequence of the hygrothermal aging has been reported by the several revealed conducted studies [31, 32]. Moreover, by means of optical observation of PA6, it is reported that the formed cracks extended to the core of the sample [33].

Understanding the properties of hygrothermally aged PA6 filament is crucial for manufacturers and designers. This work focuses on studying the physicochemical and mechanical responses of PA6 filament subjected to hygrothermal aging by 20 °C air and by immersion into distilled water at 20, 50, and 70 °C for up to 1368 h. The study investigated the physicochemical and mechanical properties of FFF-processed specimens made from moisturized filaments with different periods and non-aged/dry filaments with different raster angles (0°, 45°, and 90°). Additionally, SEM observations were conducted to evaluate the fracture surface of FFF-processed moisturized filaments at different periods.

2 Material description, characterization methods, and methodology

2.1 Material and printer

This study considers the polyamide 6 (PA6) filament produced by MarkForged®. The selected PA6 filament has a density of 1.1 g/m^3, a glass transition temperature (T_g) of 45 °C, a melting temperature (T_m) of 205 °C, and a crystallization temperature (T_c) of 173 °C. Additionally, the diameter of the filament is approximately 1.75 mm (±0.01 mm). The specimens were manufactured using the German RepRap X500® 3D printer. The printer's characteristics include a printing speed range of 10–150 mm/s, a filament/nozzle diameter of 1.75 mm/0.4 mm, a maximum extruder temperature of 752 °F (400 °C) (±2%), a heated chamber temperature of 176 °F (80 °C), and a heated print bed temperature of 248 °F (120 °C).

2.2 Characterization methods

2.2.1 Dynamic mechanical thermal analysis

Dynamic mechanical thermal analysis (DMTA) was conducted on the filament and the printed specimens to evaluate the evolution trend of the related glass transition temperatures (T_g). Indeed, dry and moisturized filaments as well as the subsequently printed specimens were subjected to the DMTA. DMTA tensile and flexural tests were applied on the filament and the printed specimens, respectively. DMTA specimens were rectangular, with dimensions of $60 \times 12.9 \times 2$ mm^3. The utilized machine was DMA Q800 TA Instruments fabricated by TA Company. The multi-frequency measurements with the frequency values of 1, 5, 10, and 30 Hz, at the temperature range of − 50 to 100 °C under the liquid nitrogen, were performed. The applied amplitude and ramp values were 20 µm and 10 °C/min, respectively, for both the tensile and flexural DMTA measurements.

2.2.2 Differential scanning calorimetry

Differential scanning calorimetry (DSC) was utilized to characterize the crystallization temperature (T_c), the enthalpy of fusion (ΔH_f), and consequently to determine the crystallinity ratio (X_c). Therefore, DSC was employed to evaluate the effect of the hygrothermal aging on evolution trend of the crystallinity percentage concerning the PA6 filament (raw material) and the subsequent printed specimens. The DSC analysis was conducted with Q10 V9.0 Build 275 TA Instruments machine at the temperature range of − 50 to 250 °C. In order to conduct the DSC characterization, two ramps were performed (heating and cooling) at a rate of 10 °C per minute for the heating and cooling steps.

2.2.3 Fourier transform infrared spectroscopy

This technique allows to identify the functional chemical groups of the material and to evaluate the occurred shift due to the hygrothermal aging process. The dry PA6 filament and the moisturized filaments in distilled water − 20 °C and 70 °C and air 20 °C were studied. FTIR measurements were performed utilizing PerkinElmer FTIR Spectrometry Frontier equipment equipped with an ATR (attenuated total reflection) accessory with a ZnSe crystal. The spectrum of each sample was performed at room temperature utilizing 16 analyses and a resolution of 4 cm^{-1}.

2.2.4 Quasi-static tensile test

The purpose of the test was to evaluate the effect of hygrothermal aging on the mechanical behavior of the specimens. The tensile test was conducted on both the dry and moisturized PA6 filament, as well as the printed specimens, using an INSTRON 5966 tensile machine equipped with a 10 kN cell and a displacement rate of 5 mm/min. Figure 3 shows the geometry of the printed specimens.

2.2.5 Microscopic observation

The microscopic observations were performed with scanning electron microscopy (SEM). The utilized SEM was HITACHI 4800 SEM high resolutions (better than 1 nm). SEM was utilized for qualitative observation of the fracture

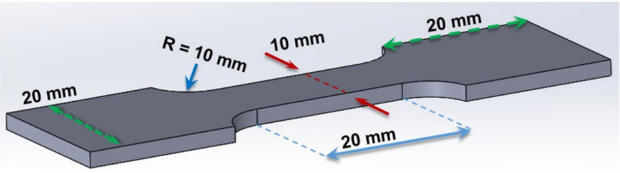

Fig. 3 Tensile specimen geometry

surface of the printed specimens. Indeed, the effect of the absorbed moisture during the different imposed hygrothermal process periods on the quality of the deposited layers of the related FFF-processed specimens was investigated. The order and quality of the deposited layers are the influencing phenomena on the strength of the FFF-processed specimens.

2.3 Methodology

Hygrothermal aging was conducted at various temperatures: 20 °C in air and 20 °C, 50 °C, and 70 °C submerged in distilled water for up to 1368 h. The investigation evaluated the percentage of absorbed water, as well as various physicochemical and mechanical properties. Four aging periods, referred to as "states of study," were defined to manufacture related specimens from the hygrothermally aged PA6 filament. The PA6 filament raw material was submerged in distilled water at 70 °C for 24, 223, and 727 h to print specimens. The specimens printed with wet filament were compared to those printed with dry filament. DMTA and tensile tests were conducted on all specimens. The specimens were characterized using DMTA with a raster orientation of 90°. For the tensile test, the specimens were printed with different raster orientations of 0°, 45°, and 90° (Fig. 4). For the tensile test, the specimens were printed with different raster orientations of 0°, 45°, and 90° (Fig. 4). The following process parameters were used for printing the tensile test specimens: print speed of 900 mm/min, layer height of 0.1 mm, bed temperature at room temperature, nozzle temperature of 240 °C, and chamber temperature at room temperature.

3 Results and discussions

3.1 Hygrothermal aging of filament (raw material)

3.1.1 Mass evolution

Based on the defined experimental design, all samples were mass weighed after undergoing a period of aging up to 1368 h concerning the temperature values of 20 °C in air (room temperature), 20 °C and 50 °C submerged in the distilled water, and also 840 h concerning 70 °C submerged in the distilled water. These measurements were utilized to determine the mass of absorbed water as the function of time and applied temperature by applying the following equation:

$$M_t(\%) = \frac{m_t - m_0}{m_0} x \tag{1}$$

where m_t and m_0 denote the mass of the sample at the given time t (which represents the duration of hygrothermal aging) and the mass of the sample before aging, respectively.

Figure 5 shows the change in the mass of absorbed moisture in the PA6 filament over time. The water uptake curves of the different filaments exhibited similar trends, regardless of the aging temperature. The moisture content increased rapidly for all samples and was proportional to the immersion time. The increase is generally associated with the diffusion of water molecules in the amorphous regions of the semi-crystalline PA6 polymer. This explains the rapid absorption of water in the early stages until saturation.

The rate of water absorption is related to the applied temperature. Therefore, an increase in the aging temperature accelerated the penetration of water into the material.

3.1.2 Evolution of the physical–chemical behaviors of the filament

To evaluate the effect of moisture penetration in PA6 filament on the glass transition temperature (T_g) over time,

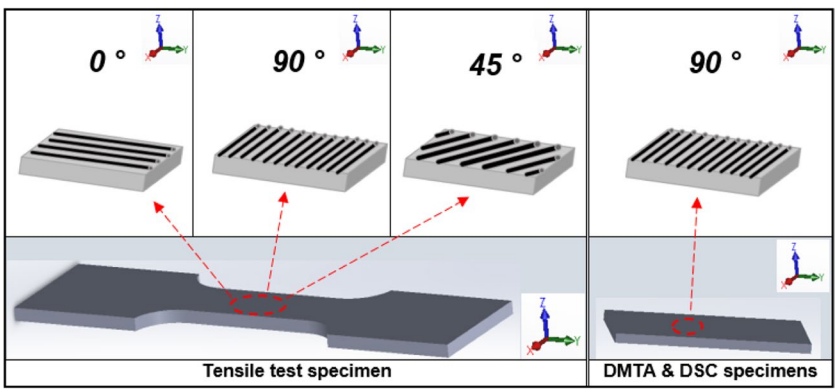

Fig. 4 Specimens concerning the tensile, DMA, and DSC tests

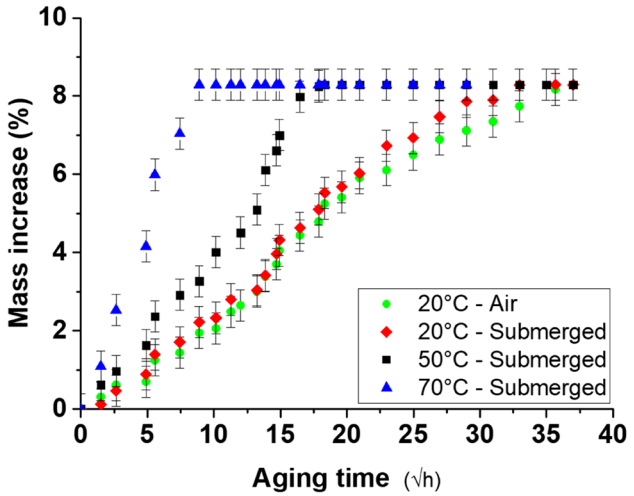

Fig. 5 Water uptake curves concerning PA6 filament

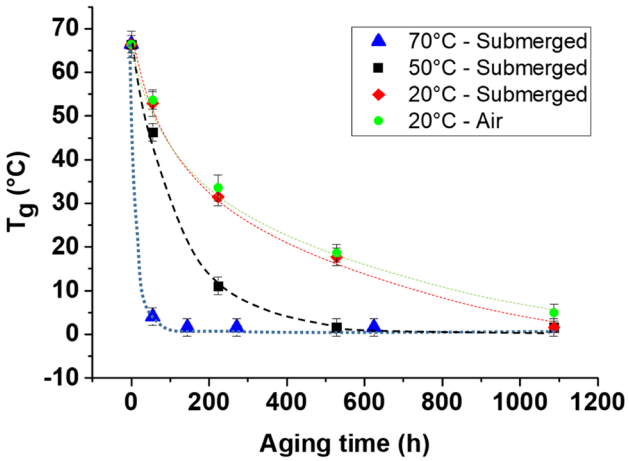

Fig. 6 Glass transition temperature evolution of PA6 filament

dynamic-mechanical analyses (DMTAs) were conducted. The DMTA analysis was performed on both non-aged and aged filaments after exposure to air at 20 °C (room temperature) for 55, 223, 528, and 1087 h, as well as distilled water at 20 °C and 50 °C. The language used is clear, concise, and objective, with a formal register and precise word choice. The text adheres to conventional structure and formatting, including consistent citation and footnote style. The content has not been altered beyond improving clarity and objectivity, and the text is free from grammatical errors, spelling mistakes, and punctuation errors. In addition, the aging periods for immersion in 70 °C distilled water were 55, 144, 271, and 624 h. The tan δ peak values obtained from DMTA characterization were used to determine the T_g values. The T_g evolution results for the PA6 filaments at the temperatures and values are shown below:

The glass transition temperature (T_g) of the non-aged filament was about 66.4 °C. However, due to the moisture absorption for the different temperatures and periods, the T_g was decreased to reach the stable value of about 2 °C. This reduction is attributed to the plasticizing effect, induced by the absorbed water. The phenomenon of chain scission that can occur especially at high temperatures also contributes to this degradation. Figure 6 illustrates that rate of T_g drop is faster for the higher considered aging temperature. The mobility of the polymer chains will be is intensified with higher temperatures. As the result of the PA6 filament exposure to 20 °C air and water immersion below T_g, the mobility of the polymer chains during the aging process is relatively low. As temperature increased to close and above T_g (50 and 70 °C), the mobility of the polymer chains was increased. Moreover, the H-bond formation between amide groups and the absorbed water is increased (Fig. 1), which increases the plasticizing effect in PA6, consequently.

The evolution of the melting and crystallization temperatures and the crystallinity rate of the hygrothermal aged PA6 filament were studied by DSC. The crystallinity percentage of the filaments was calculated according to the below formula:

$$X_c(\%) = \frac{\Delta H_m}{\Delta H_{100\%}} \tag{2}$$

where ΔH_m is the melting enthalpy and $\Delta H_{100\%}$ is the enthalpy of the 100% crystalline PA6 which is 188 J/g. No significant variation in melting and crystallization temperatures due to hygrothermal aging was observed. However, hygrothermal aging affected the crystallinity ratio of the PA6 filaments. It varies from 21.58 to 19.73% as is illustrated by Fig. 7.

Increased water absorption can cause swelling of the polymer matrix. Water molecules penetrate the polymer chains, causing them to swell and disrupt the regular packing of polymer chains. This interference can decrease the overall crystallinity of the material. Water molecules can act as plasticizers, reducing the intermolecular forces between polymer chains. This effect can disrupt the formation of crystalline regions by increasing the mobility of polymer chains and inhibiting their ability to form ordered structures. Hydrolytic degradation of polymer chains in the presence of water is also a factor to consider. Hydrolysis, facilitated by water molecules, can catalyze the breakdown of polymer chains, resulting in chain scission and a reduction in molecular weight. This degradation process can also contribute to the observed decrease in crystallinity of water-absorbing polymers.

The infrared spectra of dry PA6 filaments as well as the moisturized filaments in air and distilled water are presented in Fig. 8. Figure 8 depicts the effect of the hygrothermal

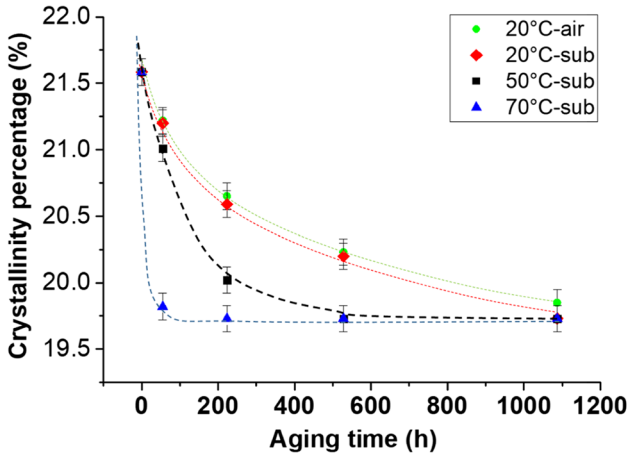

Fig. 7 Evolution of the crystallinity ratio of the PA6 filament by hygrothermal aging

aging temperature on the PA6 filaments, in the constant period of 840 h. During the imposed hygrothermal aging process, the intensity of the absorbance bands concerning most of the detected bands has evolved. Band intensities change progressively as temperature rises. So that, the peaks concerning the higher temperature (70 °C) are more highlighted. Furthermore, the effect of 20 °C distilled water was more important than 20 °C air concerning the absorbance intensity evolution of the characteristic bands during the hygrothermal aging. Some of the peaks shifted to higher frequencies (as the bonded N–H stretch and the overtone of amide II), and some of them shifted to lower frequencies (such as amide I) with aging temperature process. The observed peaks at the wavenumbers of ≈ 3490 cm^{-1} (weak at shoulder) and 3293 cm^{-1} were concerning the free N–H stretching and hydrogen-bonded N–H stretching bands, respectively [33, 34] (Fig. 8a).

As the temperature was increased, the water-absorption band intensity increased overlapping the N–H stretching band. Therefore, the free N–H stretch band absorbance is increased with temperature. The highest observed intensity of this band corresponded to the highest considered hygrothermal aging temperature (70 °C). This band is determined by an arrow. The broad absorption bands increase due to the carbonyl groups accumulated in the polymer chains resulted from the oxidation process in the range 1760–1700 cm^{-1} [33, 34] that were not highlighted in the hygrothermally aged PA6 filament in the studied temperature and periods (Fig. 8b).

3.1.3 Evolution of the mechanical behaviors of the filament

To assess the impact of absorbed moisture on the mechanical properties of the PA6 filament, we conducted a uniaxial tensile test on both non-aged and moisturised samples. This

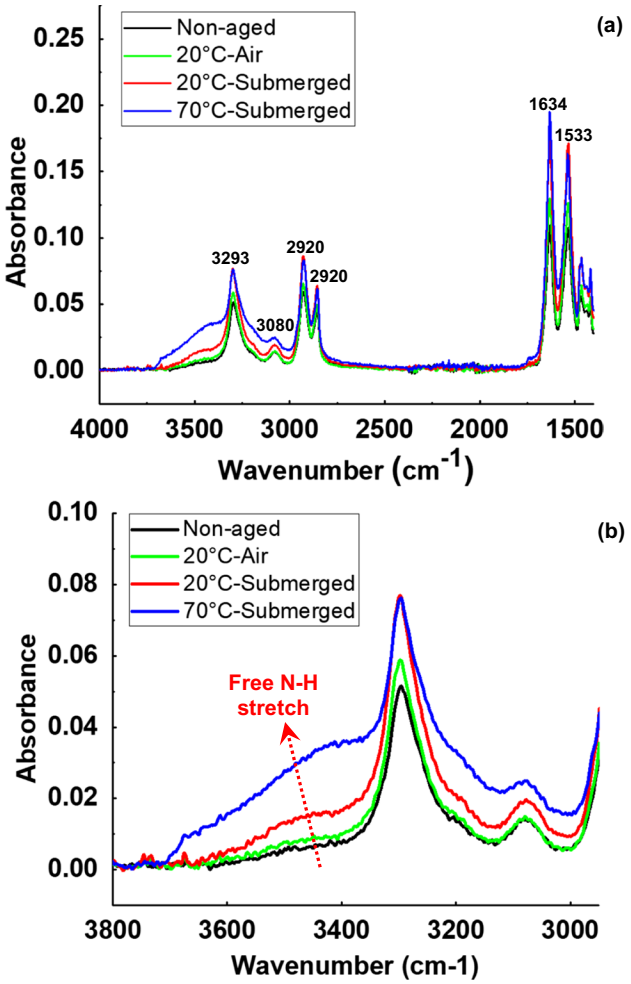

Fig. 8 Infrared spectra of non-aged/dry PA6 filaments as well as submerged in distilled water for different conditioning temperatures

test provides valuable information on the filament's tensile strength, Young's modulus, and elongation at break.

Concerning the Young's modulus, the absorbed moisture caused a reduction about 84% of the filament rigidity. The retention level of Young's modulus varies according to the applied temperature, attributed to the mass of the absorbed moisture. Figure 9 illustrated that the dramatic reduction in the rigidity of the PA6 filaments occurred in the early period of the hygrothermal aging process. Besides, the decline trend rate was more significant in the higher temperature values. The moisturized filaments at 20 °C had lower Young's modulus reduction rate. The filaments exposed to hygrothermal aging at 20 °C in air and distilled water have a close reduction trend. However, the filaments concerning the water absorption at 20 °C in the distilled water had a bit higher drop rate. This trend is correlated to the amount of the absorbed water mass (Fig. 5). Young's modulus reduction rate was faster for the filaments which had absorbed moisture with the higher rate. Therefore, the moisturized filaments

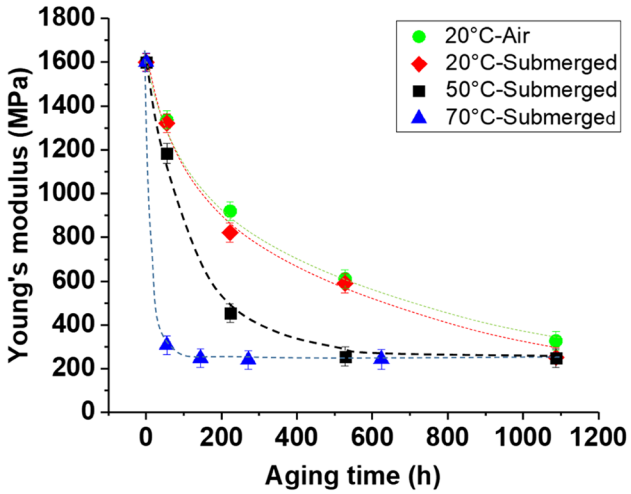

Fig. 9 Evolution of Young's modulus concerning the PA6 filaments

aged at 70 °C (the highest selected temperature value) in the distilled water exhibited the higher Young's modulus reduction rate comparing to the other selected temperature values.

Because of the presence of water in the amorphous phase of PA6 filament, the stress at yield decreases significantly, too. The absorbed moisture caused a reduction of about 85.6% of the yield stress of the PA6 filament. The representation of the curves in Fig. 10 illustrates the progression of the yield stress in various temperature conditions in response to absorbed moisture mass. An observable decline in the yield stress level of the PA6 filament was noted during the initial stages of hygrothermal aging in the different decided conditions. The filaments submerged in distilled water exhibited a more significant reduction in comparison to the hygrothermally aged filament in the 20 °C air environment in the early period of the hygrothermal aging process. The levels of yield stress exhibit a consistent trend once a specific time period has elapsed, which is contingent upon the prevailing ambient temperature. The trend towards constancy was attained at a quicker pace by the filaments which were immersed in distilled water at a temperature of 70 °C.

Moisture absorption caused a significant decrease in tensile strength of PA6 filaments. The tensile strength dropped until 45% and then reached a plateau (Fig. 11). This trend was similar to the evolution of Young's modulus. A dramatic drop in tensile strength was observed in the early stages of the hygrothermal aging process, which was shortened by the increase in moisture temperature. The rate of decrease in tensile strength of PA6 filaments immersed in distilled water at 70 °C was more significant than that of filaments exposed to moisture in a colder environment.

Figure 12 depicts the evolution of the elongation at break concerning the moisturized PA6 filaments. The moisture absorption caused the increase of the elongation at break concerning the dry PA6 filament from about 210 to 330%. Therefore, the fracture mode of the PA6 filaments was more ductile by increasing the hygrothermal aging time and temperature. Indeed, water molecules in polyamides contributed to the increase in ductility (elongation at break) by plasticizing polyamides, which softened the PA6 filaments. By increasing the temperature, the rate of the elongation at break was accelerated. This increase trend is correlated to the higher rate of the moisture absorption mass in higher temperature values (Fig. 5).

The impact of absorbed moisture on the physical–chemical and mechanical behaviors of PA6 filaments was studied to identify the effects of hygrothermal aging on printed/manufactured specimens by FFF process. The study of specimen behavior was conducted at a temperature of 70 °C. To

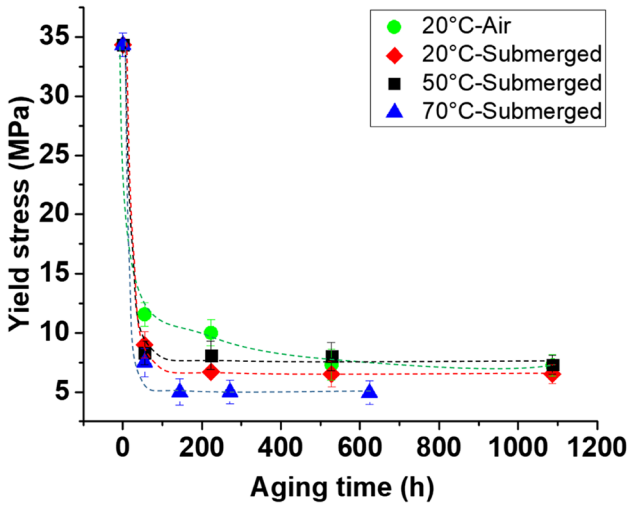

Fig. 10 Evolution of yield stress concerning the PA6 filaments

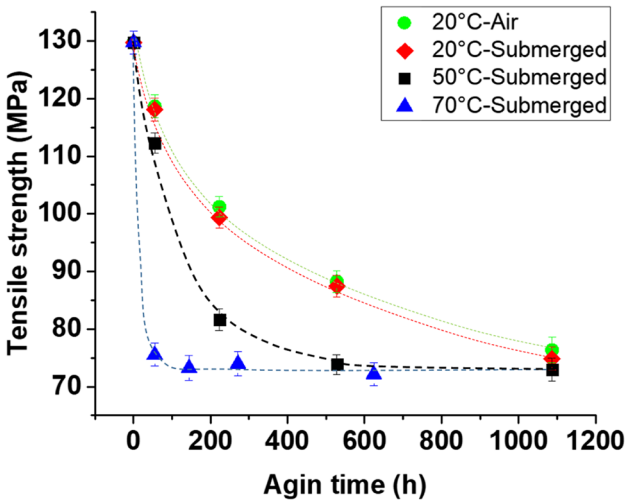

Fig. 11 Evolution of tensile strength concerning the PA6 filaments

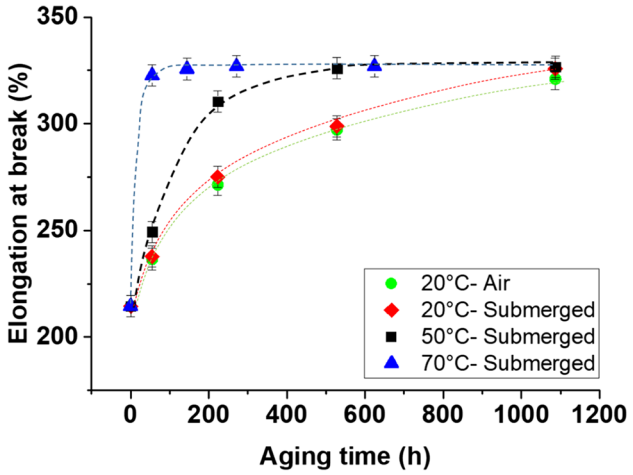

Fig. 12 Evolution of elongation at break concerning the PA6 filament

justify this decision, we compared the evolution of different properties with the mass percentage of absorbed water. For instance, Fig. 13 shows the evolution of Young's modulus with the mass percentage of absorbed moisture at different temperature values. The Young's modulus values for the moisturized PA6 filaments were found to be similar at the same absorbed moisture mass percentage, regardless of the environmental temperature.

3.2 Hygrothermal aging of the manufactured/printed specimens

In this section, the hygrothermally aged PA6 filaments in 70 °C distilled water were employed as raw material in the FFF process. Consequently, the impacts of the hygrothermally aged raw materials (filaments) on the physical–chemical and mechanical properties of the printed specimens were investigated. The considered hygrothermal aging periods were 24, 223, and 727 h. These periods were selected according to the obtained results from the conducted study on the PA6 filament (raw material) in the previous section. The main reason of the selection of these periods were to consider the different absorbed moisture mass percentages. Moreover, some specimens were manufactured with the non-aged PA6 filaments to have better observation of the effect of the moisturized filaments on the behaviors of the printed parts.

3.2.1 Dynamic mechanical analysis of the printed specimens

Dynamic mechanical analysis (DMA) analysis was conducted to identify the evolution of the glass transition temperature (T_g) of the printed specimens (Fig. 14). It can be observed that T_g of the printed specimens decreased from 68 to 51 °C after about 727 h of hygrothermal aging process. Based on this comparison between the moisturized filaments and the related FFF-processed specimens, the below observations can be listed:

- During the FFF process, the moisturized filament (as raw material) experienced a high-temperature value (about 240 °C) in the liquefier section of the FFF machine to be melted, then subsequently extruded and finally deposited layer-by-layer sequence on the bed platform. Indeed, some absorbed water in the filament was evaporated due to the experience of high temperature (about 240 °C) in the liquefier section via the FFF process. Due to this vaporization, the T_g of the printed specimens increased compared to the T_g of the filament (raw material), indi-

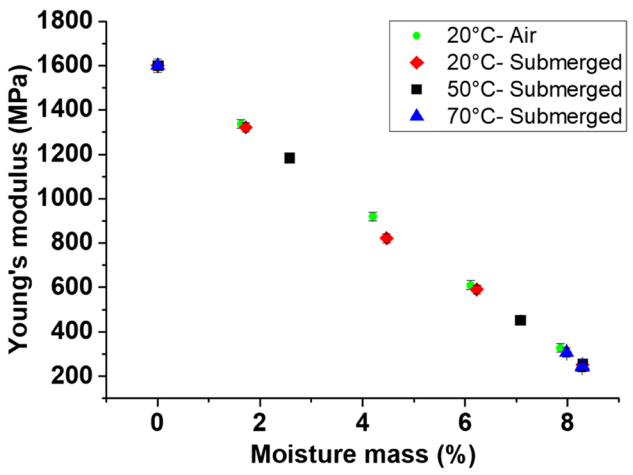

Fig. 13 Variation of Young's modulus for moisturized PA6 filaments at the different temperatures

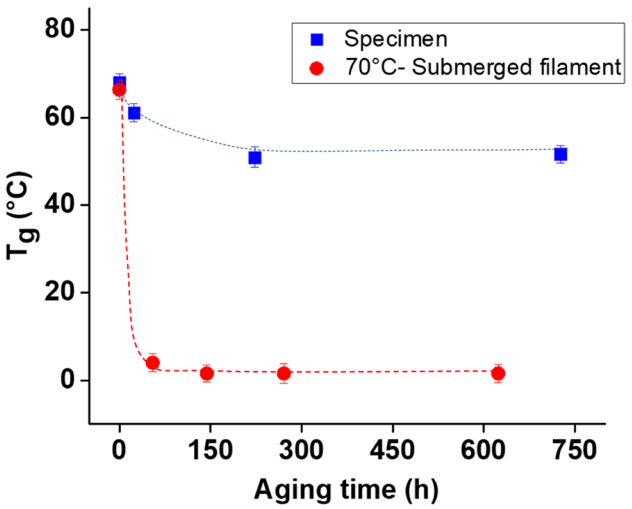

Fig. 14 Tg evolution of the printed specimens and the filaments

cating that the plasticizing effects of hygrothermal aging have a less important effect (Fig. 14). Plasticizing is considered to be a reversible aspect of the hygrothermal aging process. Furthermore, irreversible hydrolysis seems to be the main phenomenon responsible for the degradation of the printed specimens.

- The rate and height of the T_g drops were more significant in the case of the filaments compared to the printed specimens (Fig. 14).
- The amount of the absorbed moisture by the raw material (PA6 filament) did not release completely during FFF process. This note can be understood from the non-flat section of Fig. 14. Indeed, the raw materials of all the printed specimens were the moisturized PA6 filaments in the same environment (70 °C distilled water) but for different periods. Furthermore, all specimens were processed under the liquefier temperature of 240 °C, whereas their related T_g values were not identical.

3.2.2 Evolution of the mechanical properties of the printed specimens

The analysis focused on the evolution of maximum tensile stress, Young's modulus, yield stress, and elongation at break of FFF-processed specimens using moisturized PA6 filaments. The specimens were printed with raster orientations of 0°, 45°, and 90°. Figure 15 shows the evolution of Young's modulus of the manufactured specimens using moisturized filaments as raw materials for different periods and printed under different raster orientations. Young's modulus reductions were observed for all printed specimens, regardless of the printing raster orientation. Specifically, printed specimens with raster orientations of 0°, 45°, and 90° displayed reductions in Young's modulus of 24%, 38%, and 47%, respectively. The effect of moisture absorption on Young's modulus was more pronounced in the manufactured specimens with a raster orientation of 90°. The specimens manufactured with a 0° raster orientation experienced the least reduction in Young's modulus due to moisture absorption.

Figure 16 depicts the evolution of the yield stress of the printed specimens in the raster angle orientations of 0°, 45°, and 90° from the hygrothermally aged filaments for different periods. The yield stress drop is seen for all specimens The yield stress reduction of printed specimens at 0°, 45°, and 90° raster orientations were 72%, 64.7%, and 34%, respectively. Therefore, the experimental results indicated that the specimens manufactured at 0° exhibited the most notable decrease in yield stress, whereas the manufactured specimens at 90° demonstrated the least reduction in the yield stress. An intriguing observation is that the yield stress levels of the specimens were consistently stable, regardless of the raster orientation used, after a certain hygrothermal aging periods of the raw materials (filaments) for the designated timeframe. The stable stress levels were aligned and close to each other.

Figure 17 illustrates the maximum tensile stress evolution of the manufactured specimens using moisturized filaments. Similar to the elastic modulus evolution, a decreasing trend of the maximum tensile stress value was observed in all considered raster orientations. The smallest decrease was observed for the manufactured specimens with a raster orientation of 90°, which was approximately 9%. The specimens with a raster angle of 45° showed the greatest decrease, approximately 23%. It is worth noting that the maximum stress of the manufactured specimens with raster orientations of 45° and 90° reached similar values in the

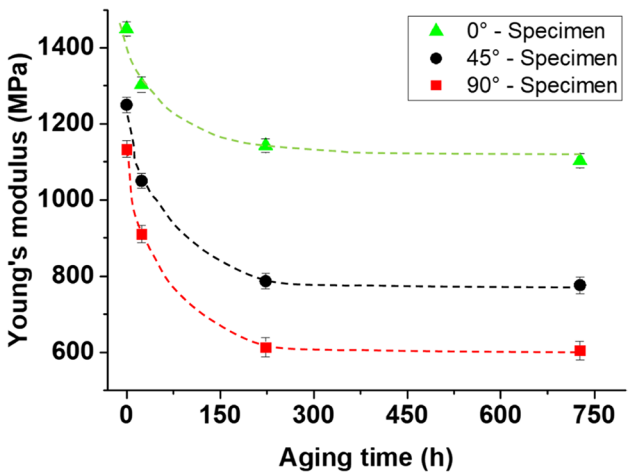

Fig. 15 Evolution of Young's modulus of the printed specimens with the moisturized raw materials in the different raster orientations

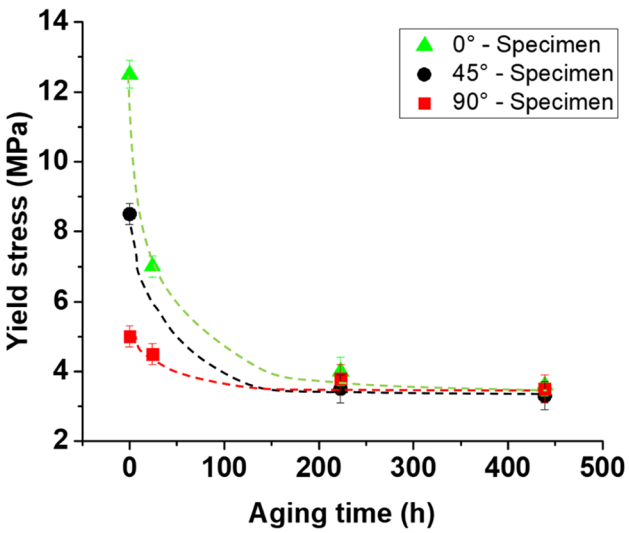

Fig. 16 Evolution of yield stress of the printed specimens with the moisturized raw materials in the different raster orientations

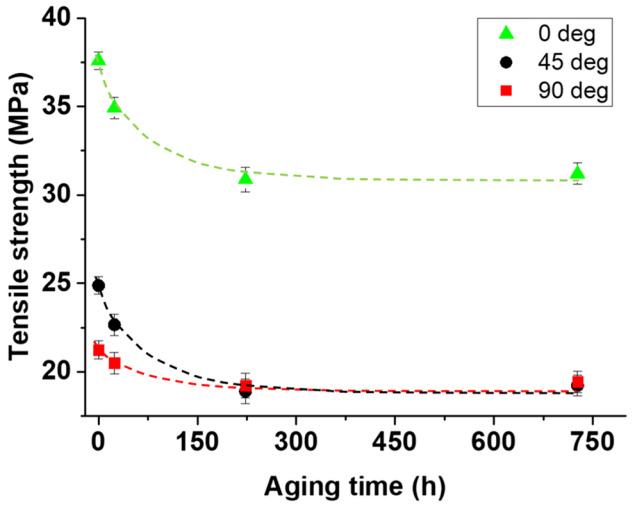

Fig. 17 Evolution of the maximum tensile stress of the printed specimens with the moisturized raw materials in the different raster orientations

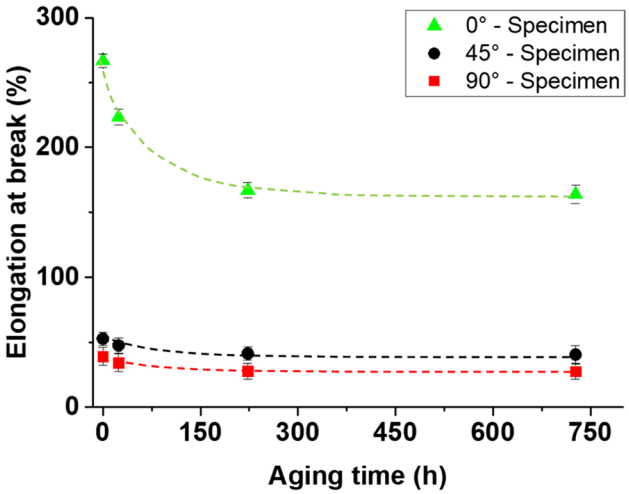

Fig. 18 Evolution of the elongation at break of the printed specimens with the moisturized raw materials in the different raster orientations

stable trend zone. The specimens manufactured with a 0° raster orientation displayed a decrease of about 17%.

The elongation at the break point of the manufactured specimens with the above-stated raster orientations decreased until the same stable values for all specimens. Indeed, the manufactured specimens with the raster orientations of 0°, 45°, and 90° displayed the decreases of about 38.6%, 23%, and 29.6%, respectively (Fig. 18). Therefore, the highest decrease is concerning 0° specimens, while the lowest decrease is concerning 45° specimens. The reduction concerning the elongation at break as the consequence of hygrothermal aging was more significant in the printed specimens with the raster orientation of 0°. Moreover, 0° specimens displayed higher values of elongation at break comparing to 45° and 90° specimens printed with the same aged filament. This is due to the different stress concentration zones in the 0° specimens and 90° specimens during the performed tensile test. For the 90° specimens, stress concentrations were at the interfaces of deposited rasters perpendicular to the applied stress orientation during tensile tests and generally weak zones as an intrinsic feature of FFF-processed objects. However, the stress concentration location in the 0° specimens was along the deposited rasters which were in the direction of the applied stress during the tensile test.

Moreover, the manufactured specimens by FFF exhibited a reduction in the elongation at break compared to the hygrothermally aged filaments (Figs. 12 and 18). The initiation of the polymer damage may have caused the observed elongation reduction in the printed specimens compared to the aged filaments (raw material). Indeed, the absorbed moisture in the hygrothermally aged filaments performed as the plasticizer. However, the moisturized filaments during the FFF process experienced a high temperature in the liquefier section (about 240 °C) which accelerated the hygrothermal aging process. The situated chain segments in the amorphous phase and connecting crystalline lamellae might be unwound and drawn due to the affected entanglement network [35]. Therefore, the plasticizer effect was no longer the predominant degrading effect, and it is most likely that the polymer has undergone hydrolysis [36, 37]. Consequently, it is well established that hygrothermal aging results in the reduction of the elongation at break of the FFF-processed specimens compared to the hygrothermally aged filaments.

3.3 Microstructures observations

To evaluate the effects of the hygrothermal aging process on the fracture characteristics of the FFF-processed specimens, the fractography of the specimens was performed with SEM (Fig. 19). Figure 19 depicts the deposited layers of a 90° specimen and shows the impact of the hygrothermal aging process on the filaments (raw materials) on the quality of the deposition during printing. It illustrates that as the period of absorption during ageing increases, the quality of the layer deposition decreases. Indeed, the specimen printed with the non-aged filament (0 h) (Fig. 19a) shows better deposition quality compared to the other aging periods of 223, 439, and 727 h. Furthermore, specimens printed with the longest-aged filament (727 h) (Fig. 19d) exhibited a lower quality of the polymer layer deposition during FFF process.

In this below section, the effect of the decrease in layer deposition quality on the mechanical properties of the post ageing printed parts is discussed. Figure 20 illustrates the superposition of the stress–strain curves concerning the 90° FFF-processed specimens with the non-aged filaments

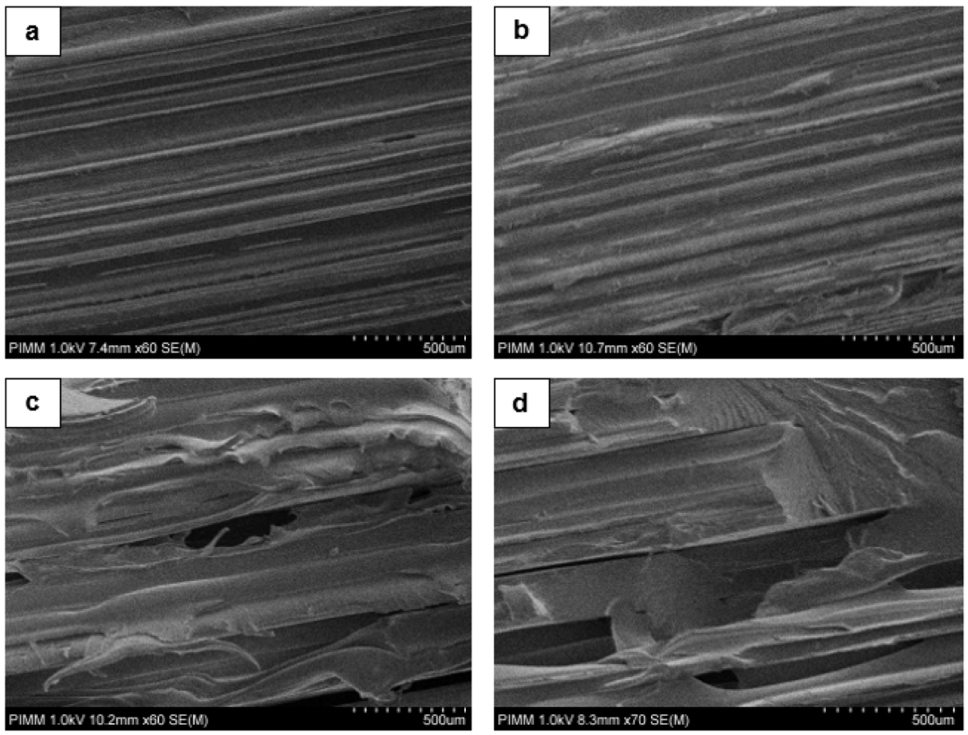

Fig. 19 The fracture surface of the 90° FFF-processed specimens concerning the dry PA6 (**a**) and the moisturized PA6 filaments during 223 h (**b**), 439 h (**c**), and 727 h (**d**) in 70 °C distilled water

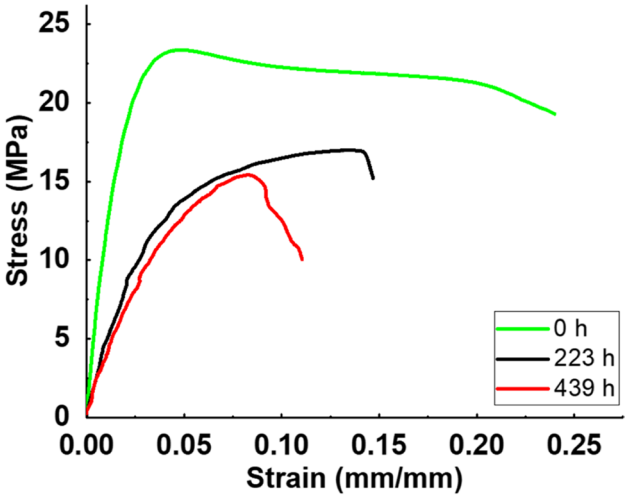

Fig. 20 Stress–strain curves concerning the 90° FFF-processed specimens with the non-aged as well as the moisturized filaments during the hygrothermal aging process periods of 223 and 439 h

and the moisturized filaments during the hygrothermal aging process periods of 223 and 439 h. The significant reduction in Young's modulus, tensile strength, and elongation at break concerning the FFF-processed PA6 specimens was observed after immersion of the raw materials in the distilled water for several hours (223 h) (Fig. 20). The obtained mechanical performance decrease of the FFF-processed specimens with the increase of the hygrothermal aging periods is correlated to the observed decrease of the deposited layer quality in Fig. 19.

3.4 Effect of hygrothermal aging on the surface quality of the FFF-processed objects

This section investigates the impact of absorbed moisture during the hygrothermal process of the PA6 filament, used as raw material, on the subsequent surface finish accuracy of the FFF-processed object. A cube with a specific geometry was manufactured using a 727-h moisturized PA6 filament and compared with another cube manufactured using dry PA6 filament (Fig. 21). Figure 21b highlights the superior surface quality of the object manufactured with dry raw material compared to the one manufactured with moisturized raw material. The protrusions from the surface and wall of the structure made with moisturized PA6 filament are depicted in Fig. 21b. These protrusions are the extruded raster from the nozzle. Simultaneously with the molten PA6 from the nozzle tip, the steam formed by absorbed moisture in the raw material was extruded. The steam flow disrupted the deposition of the PA6 rasters, preventing them from depositing on the intended sections of the object geometry.

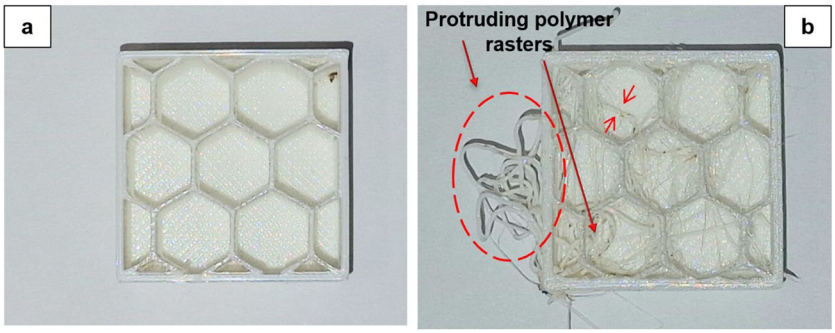

Fig. 21 FFF-processed objects with the dry (**a**) and the moisturized PA6 filaments (**b**)

4 Conclusion

This paper examines the use of PA6 filament as FFF printing feedstock and evaluates the impact of various hygrothermal aging conditions on its physicochemical, thermomechanical, and mechanical properties. The water uptake reached the same plateau value for all aging temperatures, but the absorption kinetic increased with temperature. The inclusion of water molecules in PA6 filament resulted in increased chain mobility, leading to a reduction in the glass transition temperature, crystallinity ratio, Young's modulus, tensile strength, and yield stress. These property losses followed a similar trend: a rapid decrease in the early stages of hygrothermal aging, followed by stabilization at the same minimum value for all temperatures. Additionally, elongation at break increased by a factor of seven at the maximum temperature. The degradation phenomenon occurs at a faster rate with higher temperatures. Specimens were printed using PA6 filaments that were aged under 70 °C distilled water for four different aging periods. The physicochemical, mechanical, and microstructural properties of the specimens were characterized. The T_g decreased with the aging period of the filament, but the decrease was less than that of the filaments themselves. This discrepancy is due to the vaporization of the water molecules trapped inside the aged filament during printing. This phenomenon resulted in a decrease in the quality of layer deposition. When compared to a specimen printed with an unaged filament, specimens printed with aged filament showed a reduction in Young's modulus, yield stress, and tensile strength. These mechanical properties decrease as the aging period of the filament used for printing increases. The quality of the subsequent printed part is significantly influenced by the hygrothermal aging of the filament.

Acknowledgements We would like to express our sincere thanks to Prof. Emmanuel Richaud for their invaluable advice and support during the preparation of this paper. Their expertise was instrumental in shaping the final result.

Author contribution K. Benfriha, M. Shirinbayan, and J. Fitoussi: construct the idea. K. Benfriha, M. Shirinbayan, M. Ahmadifar, C. Penavayre, S. Nouira, and J. Fitoussi: analyzed results, draft manuscript preparation, and wrote the paper. K. Benfriha, M. Shirinbayan, M. Ahmadifar, C. Penavayre, S. Nouira, and J. Fitoussi: corrected the English and the paper format.

Data Availability The authors declare that the data and the materials of this study are available within the article.

Declarations

Consent to participate Not applicable.

Consent for publication Not applicable.

Conflict of interest The authors declare no competing interests.

References

1. Anfu Guo, Dekun Kong, Xiaoyan Zhou, He Kong, Peng Qu, Shaoqing Wang, Hongbing Wang, Yingbin Hu (2022) Method for preparing damage-resistant 3D-printed ceramics via interior-to-exterior strengthening and toughening, Addit Manuf 60, Part A
2. Chen Z, Li Z, Li J, Liu C, Lao C, Yuelong Fu, Liu C, Li Y, Wang P, He Yi (2019) 3D printing of ceramics: a review. J Eur Ceram Soc 39(4):661–687
3. Kong Dekun, Guo Anfu, Hailong Wu, Li Xunjin, Jingwen Wu, Peng Qu, Wang Shaoqing (2023) Method for preparing biomimetic ceramic structures with high strength and high toughness. Ceram Intl 49(24):40284–40296
4. Ahmadifar M, Benfriha K, Shirinbayan M, Tcharkhtchi A (2021) Additive manufacturing of polymer-based composites using fused filament fabrication (FFF): a review. Appl Compos Mater 28:1335–1380
5. Ahmadifar M, Benfriha K, Shirinbayan M (2023) Thermal, tensile and fatigue behaviors of the PA6, short carbon fiber-reinforced PA6, and continuous glass fiber-reinforced PA6 materials in fused filament fabrication (FFF). Polymers 15(3):507
6. Wang X, Jiang M, Zhou Z, Gou J, Hui D (2017) 3D printing of polymer matrix composites: a review and prospective. Compos B Eng 110:442–458
7. Wu H, Fahy WP, Kim S, Kim H, Zhao N, Pilato L, Koo JH (2020) Recent developments in polymers/polymer nanocomposites for additive manufacturing. Progr Mater Sci 111:100638
8. Tofail SA, Koumoulos EP, Bandyopadhyay A, Bose S, O'Donoghue L, Charitidis C (2018) Additive manufacturing: scientific and technological challenges, market uptake and opportunities. Mater Today 21(1):22–37

9. Benfriha K, Ahmadifar M, Shirinbayan M, Tcharkhtchi A (2021) Effect of process parameters on thermal and mechanical properties of polymer-based composites using fused filament fabrication. Polym Compos 42(11):6025–6037
10. Tran TQ, Ng FL, Kai JTY, Feih S, Nai MLS (2022) Tensile strength enhancement of fused filament fabrication printed parts: a review of process improvement approaches and respective impact. Addit Manuf 54:102724
11. Daminabo SC, Goel S, Grammatikos SA, Nezhad HY, Thakur VK (2020) Fused deposition modeling-based additive manufacturing (3D printing): techniques for polymer material systems. Mater Today Chem 16:100248
12. Fico D, Rizzo D, Casciaro R, Esposito Corcione C (2022) A review of polymer-based materials for fused filament fabrication (FFF): focus on sustainability and recycled materials. Polymers 14(3):465
13. Pomes B, Derue I, Lucas A, Nguyen JF, Richaud E (2018) Water ageing of urethane dimethacrylate networks. Polym Degrad Stab 154(2018):195–202
14. Delozanne J, Desgardin N, Coulaud M, Cuvillier N, Richaud E (2020) Failure of epoxies bonded assemblies: comparison of thermal and humid ageing. J Adhes 96(10):945–968
15. Bergeret A, Pires I, Foulc MP, Abadie B, Ferry L, Crespy A (2001) The hygrothermal behaviour of glass-fibre-reinforced thermoplastic composites: a prediction of the composite lifetime. Polym Testing 20(7):753–763
16. Carrascal I, Casado JA, Polanco JA, Gutiérrez-Solana F (2005) Absorption and diffusion of humidity in fiberglass-reinforced polyamide. Polym Compos 26(5):580–586
17. Gonçalves ES, Poulsen L, Ogilby PR (2007) Mechanism of the temperature-dependent degradation of polyamide 66 films exposed to water. Polym Degrad Stab 92(11):1977–1985
18. Shinzawa H, Mizukado J (2020) Water absorption by polyamide (PA) 6 studied with two-trace two-dimensional (2T2D) near-infrared (NIR) correlation spectroscopy. J Mol Struct 1217:128389
19. Sang L, Wang C, Wang Y, Hou W (2018) Effects of hydrothermal aging on moisture absorption and property prediction of short carbon fiber reinforced polyamide 6 composites. Compos B Eng 153:306–314
20. Ishak ZM, Berry JP (1994) Hygrothermal aging studies of short carbon fiber reinforced nylon 6.6. J Appl Polym Sci 51(13):2145–2155
21. Vlasveld DPN, Groenewold JHEN, Bersee HEN, Picken SJ (2005) Moisture absorption in polyamide-6 silicate nanocomposites and its influence on the mechanical properties. Polymer 46(26):12567–12576
22. Rajeesh KR, Gnanamoorthy R, Velmurugan R (2010) Effect of humidity on the indentation hardness and flexural fatigue behavior of polyamide 6 nanocomposite. Mater Sci Eng, A 527(12):2826–2830
23. Ferreno D, Carrascal I, Ruiz E, Casado JA (2011) Characterisation by means of a finite element model of the influence of moisture content on the mechanical and fracture properties of the polyamide 6 reinforced with short glass fibre. Polym Testing 30(4):420–428
24. Puffr R, & Šebenda J (1967) On the structure and properties of polyamides. XXVII. The mechanism of water sorption in polyamides. In Journal of Polymer Science Part C: Polymer Symposia (Vol. 16, No. 1, pp. 7 9–93). New York: Wiley Subscription Services, Inc., A Wiley Company.
25. Ogunsona EO, Misra M, Mohanty AK (2017) Accelerated hydrothermal aging of biocarbon reinforced nylon biocomposites. Polym Degrad Stab 139:76–88
26. Murthy NS (2006) Hydrogen bonding, mobility, and structural transitions in aliphatic polyamides. J Polym Sci, Part B: Polym Phys 44(13):1763–1782
27. Shi K, Ye L, Li G (2015) Structure and hydrothermal stability of highly oriented polyamide 6 produced by solid hot stretching. RSC Adv 5(38):30160–30169
28. Kehrer L, Keursten J, Hirschberg V, Böhlke T (2023) Dynamic mechanical analysis of PA 6 under hydrothermal influences and viscoelastic material modeling. J Thermo Compos Mater 08927057231155864
29. Haddar N, Ksouri I, Kallel T, Mnif N (2014) Effect of hygrothermal ageing on the monotonic and cyclic loading of glass fiber reinforced polyamide. Polym Compos 35(3):501–508
30. Ksouri I, Haddar N (2018) Long term ageing of polyamide 6 and polyamide 6 reinforced with 30% of glass fibers: temperature effect. J Polym Res 25:1–12
31. Chevali VS, Dean DR, Janowski GM (2010) Effect of environmental weathering on flexural creep behavior of long fiber-reinforced thermoplastic composites. Polym Degrad Stab 95(12):2628–2640
32. Ledieu B (2010) Vieillissement en milieu eau/glycol du polyamide 66 renforce fibres de verre courtes pour l'application boite a eau de radiateur de refroidissement moteur (Doctoral dissertation, Arts et Métiers ParisTech)
33. Ksouri I, De Almeida O, Haddar N (2017) Long term ageing of polyamide 6 and polyamide 6 reinforced with 30% of glass fibers: physicochemical, mechanical and morphological characterization. J Polym Res 24:1–12
34. Okamba-Diogo O, Richaud E, Verdu J, Fernagut F, Guilment J, Fayolle B (2015) Molecular and macromolecular structure changes in polyamide 11 during thermal oxidation–Kinetic modeling. Polym Degrad Stab 120:76–87
35. El-Mazry C, Correc O, Colin X (2012) A new kinetic model for predicting polyamide 6–6 hydrolysis and its mechanical embrittlement. Polym Degrad Stab 97(6):1049–1059
36. Taktak R, Guermazi N, Derbeli J, Haddar N (2015) Effect of hygrothermal aging on the mechanical properties and ductile fracture of polyamide 6: experimental and numerical approaches. Eng Fract Mech 148:122–133
37. Phua YJ, Chow WS, Ishak ZM (2011) The hydrolytic effect of moisture and hygrothermal aging on poly (butylene succinate)/organo-montmorillonite nanocomposites. Polym Degrad Stab 96(7):1194–1203